Journal of Renewable Materials

Tech Science Press

DOI: 10.32604/jrm.2024.054905

ARTICLE

Preparation and Characterization of Hydrogel Materials Based on the Hydrothermal Liquefaction of *Enteromorpha prolifera*

Jiangyi Zhou, Bin Cao, Sivakumar Esakkimuthu, Mao Mu* and Shuang Wang*

School of Energy and Power Engineering, Jiangsu University, Zhenjiang, 212013, China

*Corresponding Authors: Mao Mu. Email: mumao@ujs.edu.cn; Shuang Wang. Email: alexjuven@ujs.edu.cn

Received: 11 June 2024 Accepted: 21 October 2024 Published: 20 December 2024

ABSTRACT

Seaweed, as a third generation of biomass energy, has significant potential to replace non-renewable fossil fuels. Among various conversion technologies, hydrothermal liquefaction can effectively convert seaweed into bio-oil. However, most current research on hydrothermal liquefaction products focuses on the oil phase and solid phase, with little attention given to the utilization of the aqueous phase by-product. In this study, the large seaweed *Enteromorpha prolifera* was selected as the raw material. The aqueous phase containing organic components was prepared through hydrothermal liquefaction at different temperatures, which was then mixed with the polymer polyvinyl alcohol to produce high-value chemical hydrogels. Furthermore, the hydrogels were salted out with Fe^{3+} to explore its influence on the degree of crosslinking. The results show that the mechanical properties of the hydrogel are optimal when the hydrothermal temperature is 160°C, with a maximum fracture stress of 0.55 MPa. After salting-out treatment, the mechanical strength of the hydrogel was further enhanced, with the maximum breaking stress increment by 1.3 times (1.26 MPa). This indicates that the process of adding the aqueous phase to the hydrogel has research potential, and Fe^{3+} can further strengthen the crosslinking process. The results of the present study will provide new insights and methods for aqueous phase valorization.

KEYWORDS

Algae biomass; hydrothermal liquefaction; volarization of aqueous phase; hydrogel

1 Introduction

The increase in fossil fuel usage has led to excessive greenhouse gas emissions, resulting in global warming. Consequently, the alternative of fossil fuel has been receiving widespread attention [1]. Biomass energy is such a feasible alternative as it is renewable and can produce liquid fuels and chemicals on a large scale [2]. So far, obtaining energy and high-value chemicals from biomass is currently the hot research topic.

In general, biomass energy has been classified into three generations. The first generation uses seeds and grains as raw materials, which yet raises many ethical concerns. The second generation uses woody biomass as raw material, which is less preferred due to its cost-ineffectiveness. The third generation involves the usage of algae biomass as a raw material, which shows many advantages, such as a short growth cycle, high yield, less land area requirement, and strong CO_2 fixation ability.

In common, algae biomass is rich in moisture, thus limiting utilization process or technology. Fortunately, hydrothermal liquefaction (HTL) is a thermochemical conversion technology that can directly use wet biomass as a raw material to produce biocrude, avoiding costly drying steps as compared to other processes. Under the HTL process, the yield of bio-oil is moderate (40%–83%) and the calorific value is considerable (28–40 MJ/kg) [3]. Although HTL technology has great potential, few researchers have paid attention to the utilization of aqueous by-products (HTL-AP) obtained after hydrothermal liquefaction. Previous studies have shown that during hydrothermal liquefaction, protein and carbohydrate derivatives tend to be dissolved in the aqueous phase, resulting in the corresponding accumulations (protein and carbohydrates) in the aqueous phase. Therefore, the aqueous phase is often rich in organic acids, cyclic amine derivatives, and N/O heterocyclic compounds [4]. Given the high content of nitrogen and oxygen-containing derivatives, HTL-AP has the significant potential for recovery and reuse [5]. At present, the recycling methods mainly include microalgae cultivation [5], anaerobic fermentation [6], hydrothermal gasification [7], etc. However, these technical means require relatively high costs, so it is necessary to develop a new and inexpensive HTL-AP value-added technology. And directly synthesizing hydrogel from HTL-AP seems to be a promising way to broaden HTL-AP utilization at a low cost.

Hydrogels are three-dimensional and hydrophilic polymer networks capable of absorbing and retaining significant amounts of water or biological fluids. Thus, they are of high moisture content, biocompatibility, and tunable physical characteristics. Most importantly, they are suitable for drug delivery, tissue engineering, wound healing, biosensors, and other applications [8]. Mechanical properties of hydrogels, such as tensible strength, are important design parameters to be considered for the engineering of hydrogels from a pharmaceutical and biomedical point of view [9]. Softer hydrogels can be used in medical fields such as drug delivery and wound dressings [10]. Harder hydrogels, due to their higher elastic modulus, can generally be used in areas such as joint scaffolds [11]. In addition, hard hydrogels can also be used as pressure sensors or in construction materials [12]. Research on hydrogels and their applications has been extensive and rapidly evolving. However, since these materials do not exhibit either solid-like behavior or liquid-like behavior, their elastic modulus values are relatively low [13]. This poses significant challenges for researchers in measuring and interpreting mechanical data. Zhou et al. introduced modified starch into polyacrylic acid to obtain hydrogels, which attained a maximum elongation rate of up to 1290%, but their maximum fracture stress was only 49.29 kPa [14]. Huang et al. considered introducing Ca^{2+} into hydrogels to enhance their mechanical properties [15]. The results showed that after the introduction of Ca^{2+}, the tensile strength of the hydrogels increased by 396.8%, reaching a maximum of 62.5 kPa. It can be seen that enhancing the tensile strength of hydrogels is one of the key focuses in current hydrogel research.

In this study, hydrogel synthesis was applied to the aqueous phase recovery. In HTL, *Enteromorpha prolifera* was selected as the raw material. Then, the aqueous phase from HTL and polyvinyl alcohol (PVA) were combined to prepare the substance-based hydrogel, so as to transform the hydrothermal aqueous phase into a high-quality hydrogel. Additionally, this study employed a salting-out method to construct a hydrogel with high mechanical strength. Compared to other aqueous phase valorization technologies, this method is cost-effective and offers significant potential for further development.

2 Materials and Methods

2.1 Materials

The used raw material is *Enteromorpha prolifera*, which is collected from the coast of Zhanjiang in the South China Sea, Guangdong Province, China. Polyvinyl alcohol PVA (the degree of polymerization is 1750 ± 50), anhydrous ethanol (analytical pure), dichloromethane (analytical pure), and anhydrous $FeCl_3$ (chemical pure) were purchased from Shanghai National Pharmaceutical Group Chemical Reagent Co., Ltd., Shanghai, China.

2.2 Water Phase Preparation of Enteromorpha prolifera

In each set of experiments, 4 g of *Enteromorpha prolifera* powder was placed into the reactor. Then, 40 mL of deionized water was added to the reactor, resulting in a solid-to-liquid ratio of 1:10. The reactor valve was then closed and sealed. The mixture was heated using a 3.0 kW electric furnace, with the target temperatures set at 160°C, 180°C, and 200°C, respectively. Once the target temperature was reached, the reaction was maintained at that temperature for an additional 30 min.

After the completion of the reaction, the reactor was allowed to cool naturally. The liquid product and solid residue from the reactor were then transferred into centrifuge tubes and initially separated using a low-speed centrifuge. Next, the liquid was transferred to a beaker and subjected to a secondary separation using a vacuum filtration apparatus. Finally, the liquid sample was extracted using dichloromethane at a volume ratio of 2:1 (dichloromethane: bio-oil). After extraction, the water phase of the organic matter from the seaweed (*Enteromorpha prolifera*) was obtained.

2.3 Hydrogel Synthesis

After obtaining the organic water phase through hydrothermal liquefaction, 3 g of polyvinyl alcohol (PVA) was added to the obtained water phase (27 g) for introducing a high molecular polymer (the concentration of PVA is 10 wt.%). Then, it was heated and stirred at 80°C for 8 h until the PVA was completely dissolved, resulting in a pre-gel solution. It is worth mentioning that no residual hydrothermal liquefaction aqueous phase or PVA was left unused. The details of the raw materials used for hydrogel synthesis are shown in Table 1.

Table 1: The raw materials used for hydrogel synthesis

Sample	Organic aqueous phase (g)	Polyvinyl alcohol (g)	Ferric chloride ethanol solution (wt.%)
E_{160}-PVA	27	3	0
E_{180}-PVA	27	3	0
E_{200}-PVA	27	3	0
E_{160}-PVA-Fe	27	3	2
E_{180}-PVA-Fe	27	3	2

The pre-gel solution is placed in a beaker and subjected to freezing treatment at a low temperature of −20°C for 12 h. The resulting hydrogel is named Ex-PVA (where x represents the hydrothermal residence temperature of *Enteromorpha prolifera*).

To explore the effect of Fe^{3+} on gel behavior, two groups of frozen samples were immersed in a sufficient volume of ferric chloride ethanol solution (with a ferric chloride concentration of 2 wt.%) [16], and further kept at −10°C for 3 days. The resulting sample was named Ex-PVA-Fe (where x represents the hydrothermal residence temperature of *Enteromorpha prolifera*).

2.4 Material Characterization

Tensile stress-strain measurement was conducted in air using a uniaxial tensile machine (WANCE) equipped with a 100 N load cell at a deformation rate of 10 mm/min. The tensile test was conducted on a universal testing machine, and the specific steps are as follows: First, the wet hydrogel was cut into strips (length 16 ± 1 mm, width 15 ± 0.5 mm, thickness 5 ± 0.5 mm). Then, the clips on the machine clamped both ends of the hydrogel strip, gradually stretching it until the hydrogel strip broke, resulting in a stress-strain curve. Infrared spectroscopy tests on the hydrogel samples are performed using the attenuated total

reflectance (ATR) method with an FT-IR spectrometer (Nicolet iS50). The morphology of the samples was observed using a scanning electron microscope (SEM) system (JSM-800, Japan). GC/MS (Agilent 7890 A/5975C, USA) was used to analyze the bio-oil composition. The ion source temperature and MS transfer line temperature were adjusted at 280°C and 60°C, respectively. Column temperature was maintained at 120°C for 5 min, then increased to 200°C at a rate of 20°C min^{-1}, and further increased to 260°C at a rate of 10°C min^{-1}, where it was maintained for 3 min. The flow rate of the carrier gas, Helium, was 1 mL min^{-1}.

3 Results and Discussion

3.1 Mechanical Strength

The stress-strain curves of the hydrogels obtained by cross-linking the organic aqueous phase with PVA are shown in Fig. 1. It can be seen from the figure that the tensile fracture stress of the hydrogel decreases initially and then increases with the rise in hydrothermal temperature. When the hydrothermal temperature is 160°C, the tensile fracture stress of the hydrogel is the highest, at 0.55 MPa. Sadeghzade et al. prepared alginate/methylcellulose hydrogels, which have a maximum fracture stress of 105.2 kPa [17]. It can be seen that the tensile strength of E-PVA has been significantly improved compared to previous studies, indicating that this process holds greater potential. As the hydrothermal temperature increases further, the maximum fracture stress withstanding capability of hydrogel decreases, which may be due to the further decomposition of macromolecular substances into small molecular organics in the aqueous phase under higher temperatures. Research shows that the mechanical strength of the hydrogel is related to the molecular weight [18]: the higher the molecular weight, the better the mechanical strength of the hydrogel. Notably, when the temperature continues to rise to 200°C, the fracture stress of the hydrogel slightly increases, which may be due to the change in the content of certain active groups in the aqueous phase.

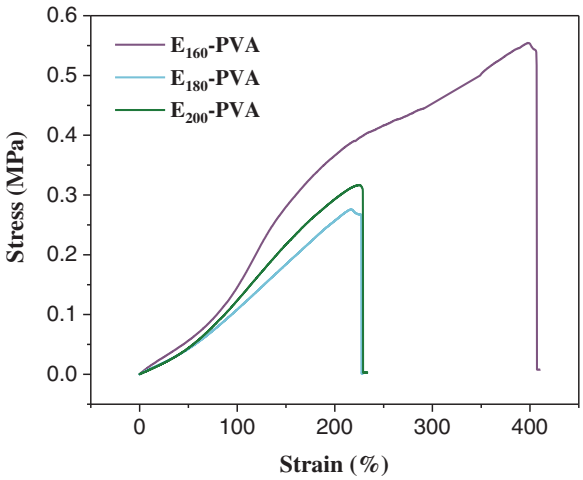

Figure 1: Stress-strain curves of E_{160}-PVA, E_{180}-PVA and E_{200}-PVA

3.2 FT-IR Infrared Testing

It is believed that the mechanical strength variation of hydrogel is ascribed to the difference of substances present in the aqueous phase from the hydrothermal process. Díaz-Vázquez et al. conducted hydrothermal liquefaction of seaweed, and the results showed the presence of organic acids, glycerol, various benzene derivatives, and nitrogen-containing compounds [19]. In addition, some studies have used microalgae as raw materials for hydrothermal liquefaction. They found that carbohydrates and protein compounds in the aqueous phase can be easily liquefied, which promotes the formation of organic

acids, amine derivatives, and N/O heterocyclic compounds [20]. Similarly, it can be inferred that the aqueous phase from hydrothermal liquefaction of *Enteromorpha prolifera* contains -COOH, -NH_2, -OH, and other functional groups. In response to this, the aqueous phase prepared at a hydrothermal temperature of 160°C was selected for GC-MS analysis in this study. The results, shown in Table A1, successfully confirmed the above inference.

In order to analyze the possible reactions of previously mentioned function groups, FT-IR tests are applied to hydrogels, and the results are shown in Fig. 2. It can be seen from Fig. 2 that E-PVA hydrogels have characteristic peaks at 3280, 2930 and 1630 cm^{-1}. The peak at 3280 cm^{-1} is attributed to the O-H bond stretching vibration, which is caused by the changes in intermolecular hydrogen bonds [21]. The peak at 2930 cm^{-1} corresponds to the N-H bond stretching vibration [22]. The peak at 1630 cm^{-1} represents the C=O bond stretching vibration in the amide II band [23]. In addition, compared to the other two hydrogels, E_{200}-PVA has an obvious characteristic peak at about 1320 cm^{-1}, which belongs to the stretching vibration peak of C-N bond [24]. This may be due to the fact that the increase in hydrothermal temperature causes organic N to migrate more into the aqueous phase. Previous studies have shown that the increase in C-N bonds will enhance the cross-linking degree of the hydrogel, which is also the reason for the rise in the fracture stress of E_{200}-PVA [25]. However, the C=O bond characteristic peak of E_{200}-PVA disappears at 1750 cm^{-1} [26], which may weaken the crosslinking effect with PVA. In contrast, the -NH bond (1230 cm^{-1}) present in E_{160}-PVA may enhance the crosslinking effect [27]. Shitrit et al. investigated the cross-linking mechanism by studying the interaction between pectin and chitosan [28]. The research results showed that the role of NH_2 groups is mainly reflected in the electrostatic interactions between molecules. In addition, it was also observed that the hydrogen bonds between the OH group of chitosan and the COOH group of pectin have also played an important role in the cross-linking process.

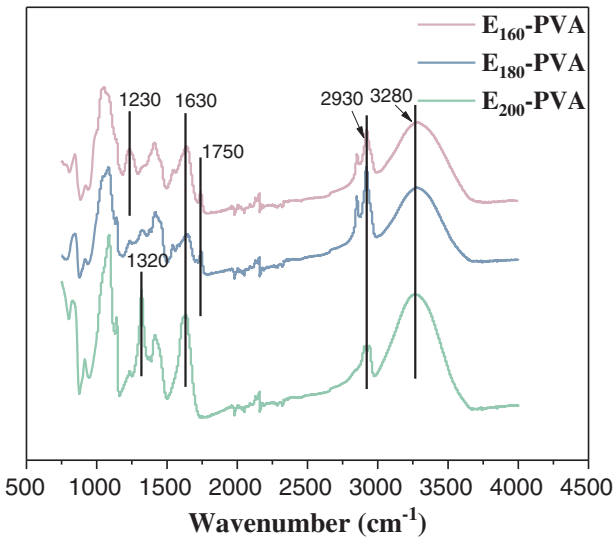

Figure 2: FT-IR spectra of E_{160}-PVA, E_{180}-PVA and E_{200}-PVA

3.3 SEM Testing

In order to further study the structure of the hydrogels, scanning electron microscopy (SEM) testing is conducted on the lyophilized hydrogels, as shown in Fig. 3. From the electron microscope image, it is evident that the surface structure of E_{160}-PVA is dense, which helps in withstanding greater stress. Conversely, the surface distribution of E_{180}-PVA appears relatively loose with numerous pores, potentially leading to a

deterioration in its mechanical properties. With the increase in hydrothermal temperature, the surface pores of E_{200}-PVA are less developed and the density falls between the first two, possibly resulting in better mechanical properties as compared to E_{180}-PVA.

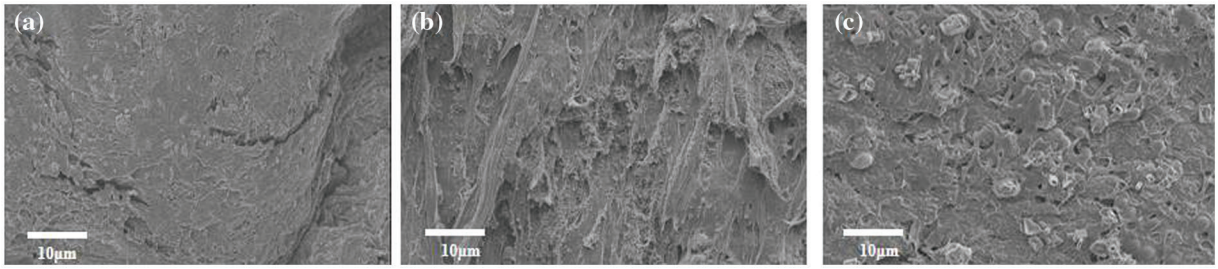

Figure 3: SEM of hydrogels: (a) E_{160}-PVA, (b) E_{180}-PVA, (c) E_{200}-PVA

3.4 The Role of Salt Precipitation Treatment

E_{160}-PVA and E_{180}-PVA were immersed in an $FeCl_3$ solution and treated by salting-out to obtain E_{160}-PVA-Fe and E_{180}-PVA-Fe, respectively. Fig. 4 illustrates the stress-strain curves of the hydrogels obtained after Fe^{3+} salting-out treatment. As depicted in the figure, the mechanical strength of the hydrogels was significantly improved after the salting-out treatment. The tensile stress of E_{160}-PVA-Fe was increased to 1.26 MPa, while that of E_{180}-PVA-Fe increased to 0.94 MPa. This enhancement was primarily obtained from the improved mechanical properties of the hydrogels resulting from electrostatic interactions between ions [15]. The mechanical properties of these ion-based interaction hydrogels can be further enhanced by adjusting the concentration of metal ions [29]. Nevertheless, compared to before the salting-out treatment, the elongation at break of the hydrogels decreased, indicating that the toughness of the hydrogels declined and they became more rigid after the salting-out treatment.

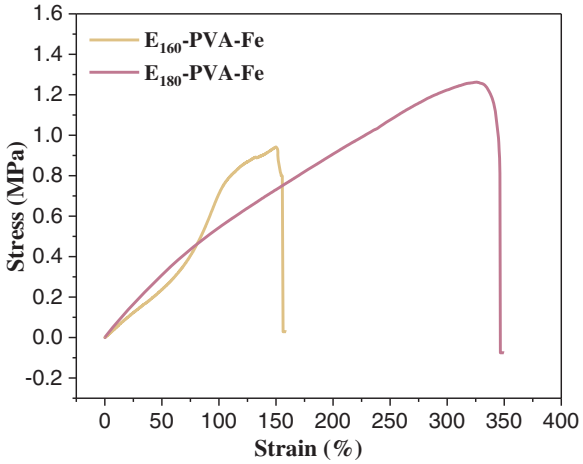

Figure 4: Stress-strain curves of E_{160}-PVA-Fe and E_{180}-PVA-Fe

Fig. 5 shows that, compared to before salting-out, the surface of the hydrogels after salting-out forms partial crystal structures and becomes denser, enhancing the mechanical strength. This is similar to previous studies. Guo et al. found that freezing combined with Fe^{3+} salting-out treatment in hydrogels led to hydrophobic aggregation in the solution and increased polymer aggregation and crystallization induced by coordination reactions, resulting in an enhanced rigid structure [16]. Their research results also

indicated that, at the microscopic level, the formation of hydrogen bonds and iron-oxygen coordination result in a honeycomb skeleton microstructure in the hydrogel samples.

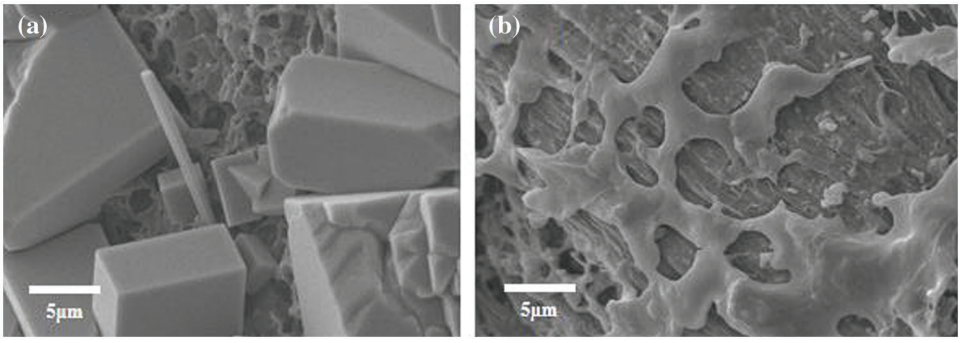

Figure 5: SEM of hydrogels: (a) E_{160}-PVA-Fe, (b) E_{180}-PVA-Fe

4 Conclusions

In summary, seaweed can be processed through hydrothermal liquefaction to obtain oil, while the by-product, the aqueous phase rich in organics, could be used to produce hydrogels by cross-linking with polymer PVA. Furthermore, treating the hydrogels with Fe^{3+} salting-out enhances the cross-linking process and significantly increases their fracture stress. The fracture stress can be raised to as high as 1.26 MPa, which is approximately a 1.3-fold increase. Thus, the present study demonstrates that Fe^{3+} optimization is highly critical in the construction of hydrogel materials with high mechanical strength. Above all, this paper indicates that the process of valorizing the aqueous phase from hydrothermal liquefaction into hydrogels with high mechanical strength is very promising.

Acknowledgement: The authors would like to express gratitude to the School of Materials Science and Engineering at Jiangsu University for providing the stress-strain testing.

Funding Statement: This work was supported by the Jiangsu Province Outstanding Youth Fund (BK20230012), the National Natural Science Foundation of China (Grant No. 52200155), the Jiangsu Funding Program for Excellent Postdoctoral Talent (2023ZB736), and the Qing Lan Project of Jiangsu Province.

Author Contributions: The authors confirm contribution to the paper as follows: study conception and design: Jiangyi Zhou, Shuang Wang; data collection: Jiangyi Zhou; analysis and interpretation of results: Jiangyi Zhou, Mao Mu, Shuang Wang; draft manuscript preparation: Jiangyi Zhou, Bin Cao, Sivakumar Esakkimuthu. All authors reviewed the results and approved the final version of the manuscript.

Availability of Data and Materials: Data will be made available on request.

Ethics Approval: Not applicable.

Conflicts of Interest: The authors declare no conflicts of interest to report regarding the present study.

References

1. Shuba Eyasu S, Kifle D. Microalgae to biofuels: ‘promising’ alternative and renewable energy, review. Renew Sustain Energy Rev. 2018;81:743–55. doi:10.1016/j.rser.2017.08.042.
2. Chisti Y. Biodiesel from microalgae. Biotechnol Adv. 2007;25(3):294–306. doi:10.1016/j.biotechadv.2007.02.001.

3. Watson J, Wang T, Si B, Chen WT, Aierzhati A, Zhang Y. Valorization of hydrothermal liquefaction aqueous phase: pathways towards commercial viability. Prog Energy Combust Sci. 2020;77:100819. doi:10.1016/j.pecs.2019.100819.
4. Chen WT, Zhang Y, Zhang J, Yu G, Schideman LC, Zhang P, et al. Hydrothermal liquefaction of mixed-culture algal biomass from wastewater treatment system into bio-crude oil. Bioresour Technol. 2014;152:130–9. doi:10.1016/j.biortech.2013.10.111.
5. Biller P, Ross AB, Skill SC, Lea-Langton A, Balasundaram B, Hall C, et al. Nutrient recycling of aqueous phase for microalgae cultivation from the hydrothermal liquefaction process. Algal Res. 2012;1(1):70–6. doi:10.1016/j.algal.2012.02.002.
6. Zheng Y, Zhao J, Xu F, Li Y. Pretreatment of lignocellulosic biomass for enhanced biogas production. Prog Energy Combust Sci. 2014;42:35–53. doi:10.1016/j.pecs.2014.01.001.
7. Lee IG, Ihm SK. Hydrogen production by SCWG treatment of wastewater from amino acid production process. Ind Eng Chem Res. 2010;49(21):10974–80. doi:10.1021/ie100469n.
8. Ho TC, Chang CC, Chan HP, Chung TW, Shu CW, Chuang KP, et al. Hydrogels: properties and applications in biomedicine. Molecules. 2022;27(9):2902. doi:10.3390/molecules27092902.
9. Vedadghavami A, Minooei F, Mohammadi MH, Khetani S, Rezaei Kolahchi A, Mashayekhan S, et al. Manufacturing of hydrogel biomaterials with controlled mechanical properties for tissue engineering applications. Acta Biomater. 2017;62:42–63. doi:10.1016/j.actbio.2017.07.028.
10. Liu H, Wang C, Li C, Qin Y, Wang Z, Yang F, et al. A functional chitosan-based hydrogel as a wound dressing and drug delivery system in the treatment of wound healing. RSC Adv. 2018;8(14):7533–49. doi:10.1039/C7RA13510F.
11. Sun Han Chang RA, Shanley JF, Kersh ME, Harley BAC. Tough and tunable scaffold-hydrogel composite biomaterial for soft-to-hard musculoskeletal tissue interfaces. Sci Adv. 2020;6(34):eabb6763. doi:10.1126/sciadv.abb6763.
12. Yang Y, Yang Y, Cao Y, Wang X, Chen Y, Liu H, et al. Anti-freezing, resilient and tough hydrogels for sensitive and large-range strain and pressure sensors. Chem Eng J. 2021;403:126431. doi:10.1016/j.cej.2020.126431.
13. Oyen ML. Mechanical characterisation of hydrogel materials. Int Mater Rev. 2014;59(1):44–59. doi:10.1179/1743280413Y.0000000022.
14. Zhou Y, Fei X, Tian J, Xu L, Li Y. Biomass-based hydrogels with high ductility, self-adhesion and conductivity inspired by starch paste for strain sensing. Int J Biol Macromol. 2022;222:1211–20. doi:10.1016/j.ijbiomac.2022.09.181.
15. Huang B, Hu R, Xue Z, Zhao J, Li Q, Xia T, et al. Continuous liquid interface production of alginate/polyacrylamide hydrogels with supramolecular shape memory properties. Carbohydr Polym. 2020;231:115736. doi:10.1016/j.carbpol.2019.115736.
16. Guo X, Dong X, Zou G, Gao H, Zhai W. Strong and tough fibrous hydrogels reinforced by multiscale hierarchical structures with multimechanisms. Sci Adv. 2023;9(2):eadf7075. doi:10.1126/sciadv.adf7075.
17. Sadeghzade S, Cao J, Yang R, Li Y, Li Y, Zhang D, et al. Highly stretchable alginate/methylcellulose hydrogels for 3D bio-printing: photopolymerization approach enhancing structural integrity. Giant. 2024;18:100280. doi:10.1016/j.giant.2024.100280.
18. Wang S, Huang W, Feng Z, Tian X, Wang D, Rao L, et al. Laccase-mediated formation of hydrogels based on silk-elastin-like protein polymers with ultra-high molecular weight. Int J Biol Macromol. 2023;231:123239. doi:10.1016/j.ijbiomac.2023.123239.
19. Díaz-Vázquez LM, Rojas-Pérez A, Fuentes-Caraballo M, Robles IV, Jena U, Das KC. Demineralization of Sargassum spp. Macroalgae biomass: selective hydrothermal liquefaction process for bio-oil production. Front Energy Res. 2015;3. doi:10.3389/fenrg.2015.00006.
20. SundarRajan P, Gopinath KP, Arun J, GracePavithra K, Adithya Joseph A, Manasa S. Insights into valuing the aqueous phase derived from hydrothermal liquefaction. Renew Sustain Energy Rev. 2021;144:111019. doi:10.1016/j.rser.2021.111019.

21. Su L, Zhou F, Yu M, Ge R, He J, Zhang B, et al. Solid lipid nanoparticles enhance the resistance of oat-derived peptides that inhibit dipeptidyl peptidase IV in simulated gastrointestinal fluids. J Funct Foods. 2020;65:103773. doi:10.1016/j.jff.2019.103773.
22. Bu K, Wu S, Zhu C, Wei M. Comparative study of HG-type low-ester hawthorn pectin as a promising material for the preparation of hydrogel. Carbohydr Polym. 2022;296:119941. doi:10.1016/j.carbpol.2022.119941.
23. Haris PI, Severcan F. FTIR spectroscopic characterization of protein structure in aqueous and non-aqueous media. J Mol Catal B: Enzym. 1999;7(1):207–21. doi:10.1016/S1381-1177(99)00030-2.
24. Hu Y, Zhan Y, Xu M, Niu F, Chen Y, Yang Q, et al. One-step preparation of flexible nanocellulose-based composite hydrogel supercapacitors with high specific capacitance. Compos Sci Technol. 2022;230:109725. doi:10.1016/j.compscitech.2022.109725.
25. Wan X, Demir B, An M, Walsh TR, Yang N. Thermal conductivities and mechanical properties of epoxy resin as a function of the degree of cross-linking. Int J Heat Mass Transf. 2021;180:121821. doi:10.1016/j.ijheatmasstransfer.2021.121821.
26. Mansur HS, Sadahira CM, Souza AN, Mansur AAP. FTIR spectroscopy characterization of poly (vinyl alcohol) hydrogel with different hydrolysis degree and chemically crosslinked with glutaraldehyde. Mater Sci Eng C. 2008;28(4):539–48. doi:10.1016/j.msec.2007.10.088.
27. Zhang P, Yuan L, Zeng J, Zou K, Liu B, Qing T, et al. Alginate production of Pseudomonas strains and its application in preparation of alginate-biomass hydrogel for heavy metal adsorption. Int J Biol Macromol. 2022;222:1511–21. doi:10.1016/j.ijbiomac.2022.09.252.
28. Shitrit Y, Bianco-Peled H. Insights into the formation mechanisms and properties of pectin hydrogel physically cross-linked with chitosan nanogels. Carbohydr Polym. 2021;269:118274. doi:10.1016/j.carbpol.2021.118274.
29. Xu J, Zhu X, Zhao J, Ling G, Zhang P. Biomedical applications of supramolecular hydrogels with enhanced mechanical properties. Adv Coll Interface Sci. 2023;321:103000. doi:10.1016/j.cis.2023.103000.

Appendix A

Table A1: List of organic components in the aqueous phase

No.	Compounds	RT. (min)	Formula	Relative content (area %)
1	Oxalic acid	10.158	$C_2H_2O_4$	6.387
2	Ammonium acetate	10.58	$C_2H_7NO_2$	5.304
3	2-Propanone, 1-hydroxy-	11.349	$C_3H_6O_2$	8.767
4	2-Propenoic acid	12.542	$C_3H_4O_2$	10.808
5	Ethylamine, 1-methyl-2-(5-methyl-1H-pyrazol-3-yl)-	14.14	$C_7H_{13}N_3$	1.229
6	3(2H)-Furanone, dihydro-2-methyl-	14.902	$C_5H_8O_2$	1.258
7	Pyrazole-4-carboxaldehyde, 1-methyl-	15.299	$C_5H_6N_2O$	4.734
8	2-Aminoimidazole-5-propionic caid	15.661	$C_6H_9N_3O_2$	3.294
9	2-Furancarboxaldehyde, 5-methyl-	16.442	$C_6H_6O_2$	8.466
10	Z-3-Methyl-2-hexenoic acid	17.838	$C_7H_{12}O_2$	2.972
11	Acetic acid, [(aminocarbonyl)amino]oxo-	18.206	$C_3H_4N_2O_4$	0.751

(Continued)

Table A1 (continued)

No.	Compounds	RT. (min)	Formula	Relative content (area %)
12	Furaneol	18.323	$C_6H_8O_3$	2.821
13	Furan-2-carbohydrazide, N2-(3-indolylmethylene)-	18.947	$C_{14}H_{11}N_3O_2$	0.541
14	2-Hydroxy-gamma-butyrolactone	19.053	$C_4H_6O_3$	0.647
15	D-glycero-D-manno-Heptitol	19.545	$C_7H_{16}O_7$	1.473
16	3,3-Dimethyl-4-methylamino-butan-2-one	20.249	$C_7H_{15}NO$	1.847
17	3-(Prop-2-enoyloxy)tetradecane	21.837	$C_{17}H_{32}O_2$	1.113
18	Uramil-N,N-diacetic acid	22.174	$C_8H_9N_3O_7$	1.167
19	2-Amino-4-dimethylaminomethylenepentanedinitrile	22.654	$C_8H_{12}N_4$	1.785
20	Methyl 2,4-di-O-methyl-β-d-xylopyranoside	23.107	$C_8H_{16}O_5$	4.198
21	l-Gala-l-ido-octose	23.446	$C_8H_{16}O_8$	0.876
22	2,4-Di-tert-butylphenol	23.809	$C_{14}H_{22}O$	2.902
23	Tetrahydro-4H-pyran-4-ol	24.233	$C_5H_{10}O_2$	0.840
24	Ethyl 2,3-epoxybutyrate	24.506	$C_6H_{10}O_3$	15.863
25	Ethyl 2,3-epoxybutyrate	24.984	$C_6H_{10}O_3$	7.963
26	1,4-diazabicyclo[4.3.0]nonan-2,5-dione, 3-methyl	30.594	$C_8H_{12}N_2O_2$	1.353
27	Tricyclo[4.3.1.1(3,8)]undecane-3-carboxylic acid	31.704	$C_{12}H_{18}O_2$	0.640